OUT-OF-PLANE ANALYSIS OF DRY-STONE WALLS USING A PSEUDO-STATIC EXPERIMENTAL AND NUMERICAL APPROACH IN SCALED-DOWN SPECIMENS

Sandra Santa-Cruz[1], Dominique Daudon[2], Nicola Tarque[1], Criss Zanelli[1], and Julio Alcántara[1]

ABSTRACT

The objective of the present work is to study the response of dry stone walls subjected to out-of-plane forces and the influence of block`s rugosity, joint arrangement, and border conditions. For this purpose, a series of scaled-down experimental tests on a tilting table and 3D numerical modelling using discrete elements, DEM, are proposed. In the numerical model, the applicability of some types of discrete elements is first studied. The preliminary analysis gives us useful information about the effects of the joint disposition and the border conditions in the response. Finally, the sensitivity of the response of the blocks to the parameter's variations is analyzed. The experimental and numerical results show that the DEM method is adequate to simulate the failure mode, the displacement, and the lateral load of stone walls due to out-of-plane lateral loads considering the effect of the irregularity of the blocks, joint arrangement, and border conditions.

Keywords: Masonry, numerical modelling, walls, DEM, YADE, earthquake, tilting table

[1] GERDIS Research Group, Engineering Department, Pontificia Universidad Católica del Perú

[2] Lab 3rs Grenoble University

1. Introduction

Dry Stone Walls, DSW, are handmade walls without mortar in their joints. Nowadays, DSW is found in heritage constructions in Europa, Africa, Asia [1], and South America [2]. Some of these constructions are located in high seismicity regions, and they are prone to in-plane and out-of-plane failure. The lack of restrictions in this direction due to excessive distances between supports or inadequate connection, or the lack of rigid floor, increases the out-of-plane failure risk in masonry buildings. Mechanisms and load factor equations for overturning failures can be found in [3]. Examples of the poor seismic performance of this type of buildings in past events in Italy, Greece, Turkey, Montenegro, Algeria and India are described in detail in [4].

Guidelines for the seismic analysis and evaluation of DSW assume that the walls act as gravity walls or macro-blocks [5], [6]. The advantage of these models is their simplicity; however, they cannot be used to model some types of failures reported in past events, such as delamination [4] or collapse due to high-frequency vibrations [7]. Thus, we need to study these kinds of failures with more refined models. Characterization of DSW and their capacity estimation are very challenging tasks because of the large variability in the properties of the material and the construction process.

Several authors have focused on the study of the out-of-plane capacity of DSW with analytical methods. The stability of masonry walls subjected to out-of-plane loads is investigated using the upper-bound kinematic approach [8] and a simplified kinematic limit analysis [9] to assess the ultimate failure of masonry in a yield design framework. With these theoretical methods, it is possible to estimate the ultimate horizontal load-bearing capacity of masonry structures and the failure surface. The analysis of imperfections and different arrangements have been addressed by rounding the brick's vertices in the contact area. The

suitability of analytical methods was demonstrated by experimental tests using a tilting table, as described in [8], [9], [10] and [11].

The numerical analyses of masonry walls constituted by regular, quasi-regular or irregular stone patterns are time-consuming when analyzing detailed finite element models. However, some accuracy simplifications can be found in the literature. A more updated work regarding limit analysis can be seen in [12]. Here, the authors applied a stochastic homogenization technique on several representative volume elements (RVE) to compute the in-plane and out-of-plane failure surfaces of masonry walls. This technique allows simulating the non-linear structural behavior of one stone wall combining a homogenization procedure and finite element limit analyses. According to [13], homogenization is a rational procedure with good compromising between micro and macro modeling, ending with acceptable stress-strength constitutive laws for masonry. Also, it reduces the computational cost by reducing the number of elements within a finite element model. If a stochastic procedure is added for simulating different RVE patterns within masonry walls, then more accurate values of the ultimate behavior of masonry walls can be computed. This approach seems to be very advantageous for the reduction of computational costs but it has only been applied to static loads.

Regarding the numerical methods, the Discrete Element Method (DEM) [14] is suitable for reproducing the mode of failure, the crack propagation pattern [15] and the failure angle [16] of brick masonry specimens, previously tested in tilting tables. It has also been numerically demonstrated that the slenderness and the block arrangement in the masonry are fundamental for the stability of the DWS [17]. All of these studies have analyzed models with regular blocks and ideal border conditions, which could produce unreal strong interlocking between blocks in 3D models [18]; then, micro-gaps between the vertical joints of the models should

be introduced to avoid this effect. To represent rugosity or roughness between blocks in full-scale specimens, DEM`s blocks may be modelled as hollow clumps of particles [19]. Although this strategy gave a good fit between experimental and numerical results (collapse loads), the study is limited to a two-dimensional field (2D model). DEM has also been used to modeling the seismic behavior of masonry structures [20],[21],[22], showing the influence of the predominant frequency on the collapse mechanism.

This work is the first stage of a research project which aims to evaluate the earthquake performance of DSWs. In this first stage, we used a pseudo-static analysis as a preliminary approach to a dynamic problem. The study presented here relies on a set of 9 down-scale pseudo-static experimental tests and numerical analysis to verify the DEM adequacy to simulate the mode of failure and the response in terms of displacement and capacity of DSW subjected to out-of-plane loads. We analyze the influence of the irregularity of the blocks, the arrangement of the blocks, and the effect of restraining conditions. The tests are pseudo-static and monotonic, and gravity loads are induced in the out-of-plane direction of the specimens by the rotation of a tilting table until the collapse of the wall specimen.

The incidence of the type of arrangement of blocks: continuous, discontinuous, and irregular-random are analyzed through a full-scale, tridimensional, numerical model (3D model) made of prismatic blocks. We also estimated the response for different height-longitude ratio. The software 3DEC V4.2 [23] was used for these analyses.

To model the down-scale experimental specimens, different types of DEM elements were considered to identify the one that can represent the geometry and the relative movement of the blocks with a reasonable computational time-cost. Then, contact forces parameters of the numerical models are calibrated so that theoretical collapse angles match the experimental

ones. Finally, the effect of lateral restrictions on the drifts and collapse angle is studied. To do so, we used the software YADE v1.20.0 [24].

2. Experimental tests

2.1 Specimen

The study focuses on a DSW that has 1.5 m height, 6 m length, a trapezoidal cross-section, and a slender ratio (height/width) of 3.3 on average, which are the dimensions of typical constructions in real suburbs construction in Latin America [25]. In total, 9 down-scale specimens (1:4) were built with cobblestone and stone blocks. The first ones have regular prismatic blocks while the others have a slightly irregular shape. The properties of the specimens are shown in Table 1 and the dimensions of the cross-section in Figure 1.

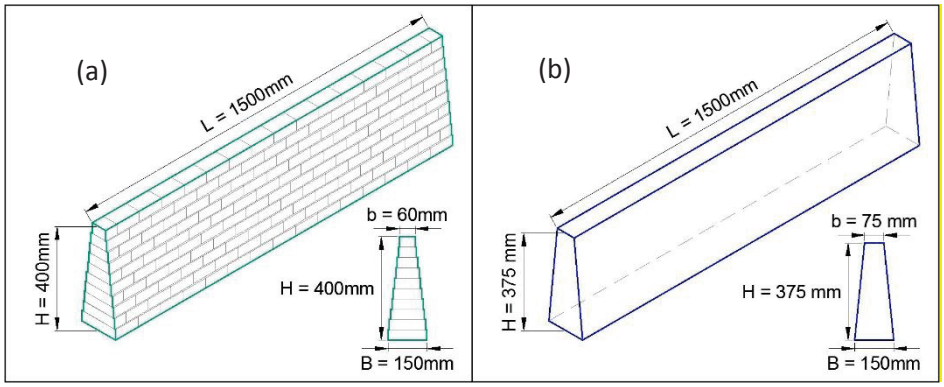

Figure 1: Cross-section and general view of 1:4 specimens built with (a) cobblestone and (b) stone blocks

The base of the specimens was restrained with two wooden pieces, to avoid sliding failure. Joints in cobblestone walls are discontinuous (Figure 2a); and in stone walls, irregular (Figure 2b). Irregular joints depend on the block's shape and the construction process. Wedge-shaped stones were placed between some blocks to avoid block relative rotation in stone walls.

Table 1: Characteristics of the tested specimens

Specimens	CBL1, CBL2, CBL3	SBL1, SBL2, SBL3	SBR1, SBR2, SBR3
Block	Cobblestone	Stone shaped with grinder and chisel	
Material	Concrete	Shale and limestone	
Block shape	Regular(prismatic)	Slightly irregular	
Block Dimensions	200 x 40 x 100 mm	100 mm x 50 mm x 150 mm aprox.	
Weight	1333 N	1371 N	
Porosity	4%	21%	
Joints	Discontinuous	Irregular	
Border conditions	No restriction	No restriction	Partially restrained

To simulate the border restrictions, we use a rope manually tensioned at the specimen ends (Figure 3). The length of the wall between the 2 ropes is 1.4 meters, (L/H = 3.7). In section 4 it is shown that the L/H should be less than 4 to see the effect of the restrictions in the response.

(a) (b)

Figure 2: Specimens with no restrictions at the ends (a) Cobblestone blocks CBL and (b) Stone blocks SBL

Figure 3: SBR specimen with restriction at the ends

2.2 Tests

Equipment consisting of a tilting platform was built. The platform is made of wood with dimensions 1600mm x 600mm x 40mm supported by a semicircle wooden piece that rolls manually, controlled by a lever and pulley mechanism sustained by a wooden frame (Figure 4). By rolling the semicircle, the platform tilts an angle, α, which can be measured with a protractor and spirit level. The maximum rotation angle is 45º. Similar equipment has been used in [26].

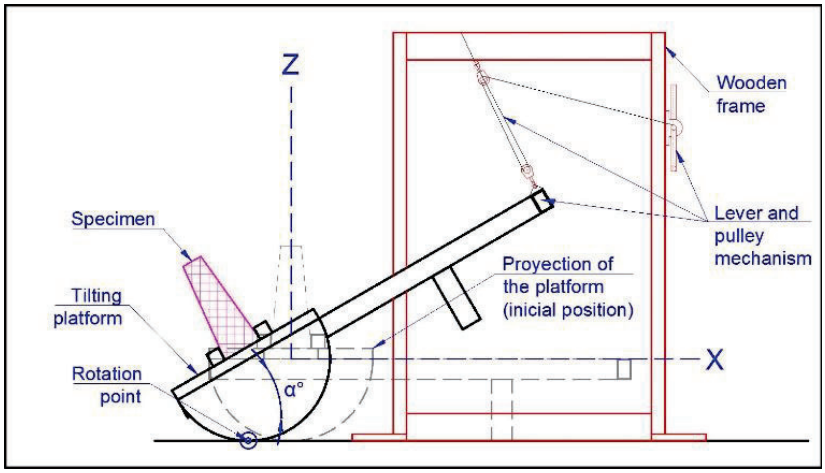

Figure 4: Scheme of the tilting table

The tests consisted of building the specimen on the tilting table to generate out-of-plane gravity loads directly proportional to the tilting angle and the weight of the wall. The test starts with $\alpha = 0$. Then, we gradually increase α, in increments of 5º and stop to record the coordinates of three-point on top of the wall (left, center and right). We used a survey equipment Pentax, model R-423 VN to measure the out-of-plane displacements. The error of the equipment is 5mm. The test continued until the collapse of the wall and the collapse angle is registered.

The walls weight can be decomposed in two directions relative to the tilted platform: the normal direction, F_v, and the out of the plane direction, F_H, as in Eq 2

$$F_V = Wsin(\alpha), F_H = Wcos(\alpha) \quad (1)$$

where W is the weight of the wall and, α is the platform angle.

The three CBL walls presented toppling of the 60% upper section. Two of them presented a uniform 2D behavior, as shown in Figure 5b. A shear deformation could be appreciated before the collapse, as seen in Figure 5a.

Figure 5: CBL tests (a) Relative displacement in blocks (b) Toppling failure

Unlike CBL, SBL irregular block shape enables the rotation of the units. Failure in SBL walls started in a random section and then it extends all along the wall (Figure 6). Failure in the three SBR walls started in the central section due to the rotation of the blocks as shown in Figure 7. This "bending" behavior, known as catenary action [27] is caused by the contact forces and the lateral restrictions.

Figure 6: Failure of SBL wall

Figurae7: Failure of SBR wall

2.3. Results

Table 2 reports the collapse angles, α_{max} measured in the tests. The CBL values are slightly lower than the critical angle as a rigid block, α_v =atan (B/H)=21.8º. On average, α_{max} of SBL specimens is 24% lower than CBL's. The lateral restrictions increase this value by 36%. Out-of-plane collapse forces, F_{VR} were estimated with Eq. 2 replacing $\alpha = \alpha_{max}$. Results show that SBR capacity is 35% greater than SBL`s. Table 2 shows the mean values, the standard deviation, σ, and the variation coefficient, COV.

Table 2. Collapse angle and out-of-plane acting forces

Specimen	α_{max}	F_{VR}/W	Specimen	α_{max}	F_{VR}/W	Specimen	α_{max}	F_{VR}/W
CBL1	19	0.33	**SBL1**	13.5	0.23	**SBR1**	18	0.31
CBL2	19	0.33	**SBL2**	14.5	0.25	**SBR2**	19	0.33
CBL3	18.5	0.32	**SBL3**	15.0	0.26	**SBR3**	21.5	0.37
Mean	18.8	0.33		14.3	0.25		19.5	0.34
σ	0.29	0.01		0.76	0.02		1.80	0.03
COV (%)	1.53	1.77		5.33	6.19		9.25	9.07

In Table 3, the out-of-plane displacements for different tilting angles for the SBL and SBR specimens are presented. In the case of SBL, the average of the out-of-plane displacements along the wall (left, center and right) is reported. For SBR, the difference of the out-of-plane displacement in the center in respect to the average displacement of the ends was calculated. It is verified that the restriction of the borders limits the displacement of the upper central

point of the wall. When the platform tilt is 5°, the displacements of SBR specimens are only 13% of the SBL`s ones. This percentage increases by up to 73% for 10°. The maximum displacement of the SBR specimen (before the collapse for 15°) is then 40% greater than the maximum displacement of the SBL wall (which failed at 10°). The displacements of the CBL specimens are not reported as they are smaller than the precision range values of the measuring instrument.

Table 3. Out-of-plane displacements for SBL (average displacement) and SBR (relative maximum at the centre) for each α

α Specimen	5°	10 °	15°	α Specimen	5°	10 °	15°
SBL1	1.9	2.9		**SBR1**	0.1	0.9	3.4
SBL2	1.2	2.0		**SBR2**	0.3	0.9	2.0
SBL3	0.9	1.7	Collapse	**SBR3**	0.2	3.1	4.0
Mean	1.3	2.2		**Mean**	0.2	1.6	3.1
σ	0.51	0.62		σ	0.1	1.3	1.03
COV (%)	38.5	28.4		**COV**	50	77.7	32.8

3. THE DEM METHOD

The DEM [8] allows to simulate the mechanical response of systems composed of blocks or discrete particles (generally rigid) by solving the equilibrium between the acting forces and the contact forces between particles. The method is iterative and starts from an initial state of the blocks assembly (position, velocity and acceleration). First, the sum of the external forces and the sub-contact forces is calculated (each contact is discretized into sub-contacts). Then, the body motion equation (2nd law of Newton) is updated by a time-numerical integration of the acceleration; for example, central difference. Damping can be introduced automatically to dissipate energy and reach the static equilibrium while computing the static state of the system with a dynamic equation. This damping is a tricky way to reach the equilibrium at the less computational cost but without real physical meaning. In a dynamic problem (such as seismic loads) the damping used is more physically defined on the Rayleigh

damping methodology over both or separately, the mass, or the stiffness [23]. After forces evaluation, the acceleration of each block is calculated from the set of forces. The block's velocity and displacement are obtained after two integrations in time. Finally, the contact forces are updated according to a chosen constitutive contact law.

This classical DEM method is an explicit scheme of integration in time and in order to assure stability and convergence, the time step should be carefully chosen. Critical time step is automatically computed by DEM algorithms (such as [23], [24]) as the compressive waves' smallest period, deduced from rigidity and mass ratio of the particles set minored by a safety factor from 20 to 100. Time step is directly related to the contact forces linearization by the concept of rigidity of contact (smooth contact type).

Non-smooth Dynamic contact type [28], implemented in the LMGC code at Montpellier university, is more suitable to consider the unilaterality of the contact physical properties than the smooth contact type. LMGC uses an implicit time integration scheme associated with convergence problems. To accelerate the convergence of the calculation, it introduces other numerical scheme types (such as small perturbations) [29], [30]. This LMGC code has been used to simulate some large historical buildings in France [31], [32].

The most widely used constitutive contact laws in the literature to represent the contact mechanism between blocks or particles come from the Coulomb model, in which the forces are proportional to the overlapping displacements of particles in contact and where the resistance is defined by the friction and the normal forces of the sub-contact.

The displacement increments are used to calculate the elastic force increments ΔF as indicated by Eq. (2).

$$\Delta F^n = -K_n \Delta U^n A_c, \Delta F_i^s = -K_s \Delta U_i^s A_c \quad (2)$$

where K_n is the proportionality factor in the normal direction, K_s is the tangential or shear direction of the joint, ΔU is the displacement increment and A_c is the sub-contact area. The superscripts *n* and *s* refer to the normal and shear directions, respectively.

The maximum shear force is defined by Eq. 3, where c and ϕ are the cohesion and the friction angle, respectively. The maximum shear force is given by Eq. 3 and refers to the historical conception of 3DEC for Soils and Rocks problems.

$$F_{max}^s = cA_c + F^n tan\phi \quad (3)$$

Figure 8 shows the interaction and the constitutive diagram for (a) normal force and (b) shear force of the sub-contacts or joints according to the Coulomb model. The relationship between the normal force and the normal displacement is perfectly elastic, while the relationship between shear force and shear displacement is elasto-plastic. The complexity of finding the sub-contact plane depends on the geometry of the iterating bodies.

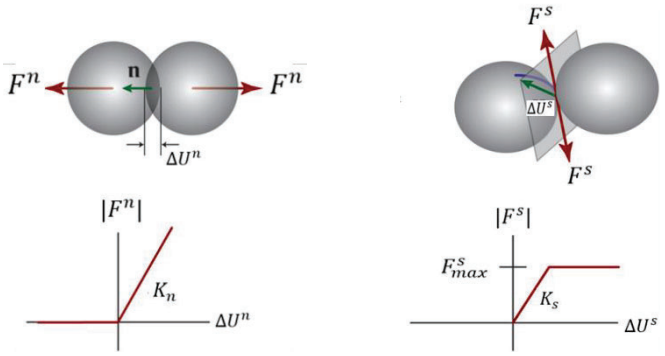

(a) (b)

Figure 8: Interaction and a constitutive diagram for (a) normal force and (b) shear force according to the Coulomb model

The DEM method has been used first for mining engineering problems by Cundall [12]. Some pioneer's works have simulated large problems for historical building by modeling these structures as a collection of separate and regular shaped blocks with cohesive or dry joints, using 3DEC code ([33], [34], [35][36], [37] and, [38]). [39] and [40], have studied both full-scale and scaled-down experimental tests on traditional masonry walls and arches. Some of the studies consider the cement joint (when existing) as an interface with more complex properties by considering tension resistance, cohesion, dilatation angle and specific rigidity. A limitation encountered is that any numerical model cannot represent uncertainties and variations of mechanical properties that are found in this type of structures. Predictive methods are largely dependent on the evaluation of these properties. In order to get over this limitation, stochastic methods can be used [41].

4. A PRELIMINARY ANALYSIS

4.1. Influence of the joints types on the displacements

In this section, the variation of the out-of-plane displacement response due to the arrangement of the joints is studied in a full-scale model. The types of arrangement are: continuous (Figure 9a), discontinuous (Figure 9b), or irregular (Figure 9c). The joints planes in the continuous and discontinuous arrangements are perfectly horizontal, while in the irregular one, the slope of the joint planes (dip angle) is randomly distributed in an interval specified by the user. DSWs are modelled with prismatic units with restricted edges with H= 1.0 m, L= 4.0 m, B= 0.45 m, and b= 0.25 m, in the 3DEC software [23]. The walls are subjected to a static trapezoidal lateral load due to service conditions to estimate the maximum out-of-plane displacement at the wall top. The values of the model parameters, shown in Table 5, correspond to the most frequent values found in the literature. The dip angle is randomly distributed in the interval [-20º, 20º].

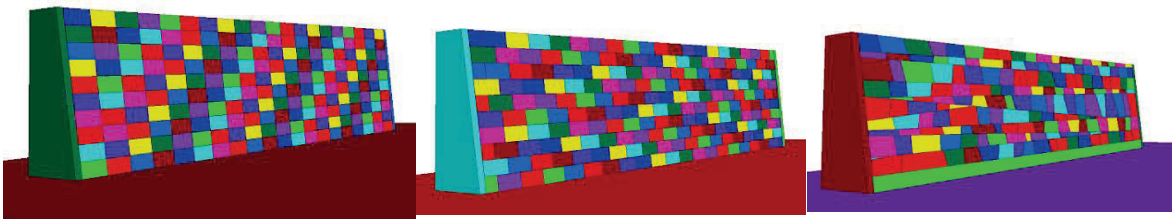

(a) (b) (c)

Figure 9: Numerical models with different types of joints: a) continuous, b) discontinuous and c) irregular

Table 5: Mechanical properties of the blocks and joints

	Parameter	Value	Units
Block	**Density**	2.40E+03	Kg/m3
	Young module	3.07E+10	Pa
	Poisson	0.18	-
Joints	**Kn**	7.5, 8.5, 9.5, 10.5, 11.5 y 12.5	x 10^7 Pa/m
	Kn/Ks	2	Pa/m
	ϕ	30	°
	c	1.00E+05	Pa
	damping	0.8	

To obtain the maximum displacement value of the model with irregular joints, 30 models were simulated with random variations in the shape and size of the blocks for different values of *Kn* (see Table 5). The average of the displacements of the DSW with irregular joints, μ, are shown in the dotted line in Figure 10. The coefficient of variation of the displacements varies between approximately 21 and 25%. Figure 10 also shows the maximum displacements due to the service loads vs K_n curves for the DSW with continuous and discontinuous joints. The highest displacement values are obtained with the discontinuous joint model for all *Kn* values. The displacements decrease by approximately 40% in the continuous joint model. The average displacements of the walls with irregular joints have values between the two values of the previous cases for each *Kn* value. The dashed line curves represent the mean values plus or minus one standard deviation of the displacements in the models with irregular joints.

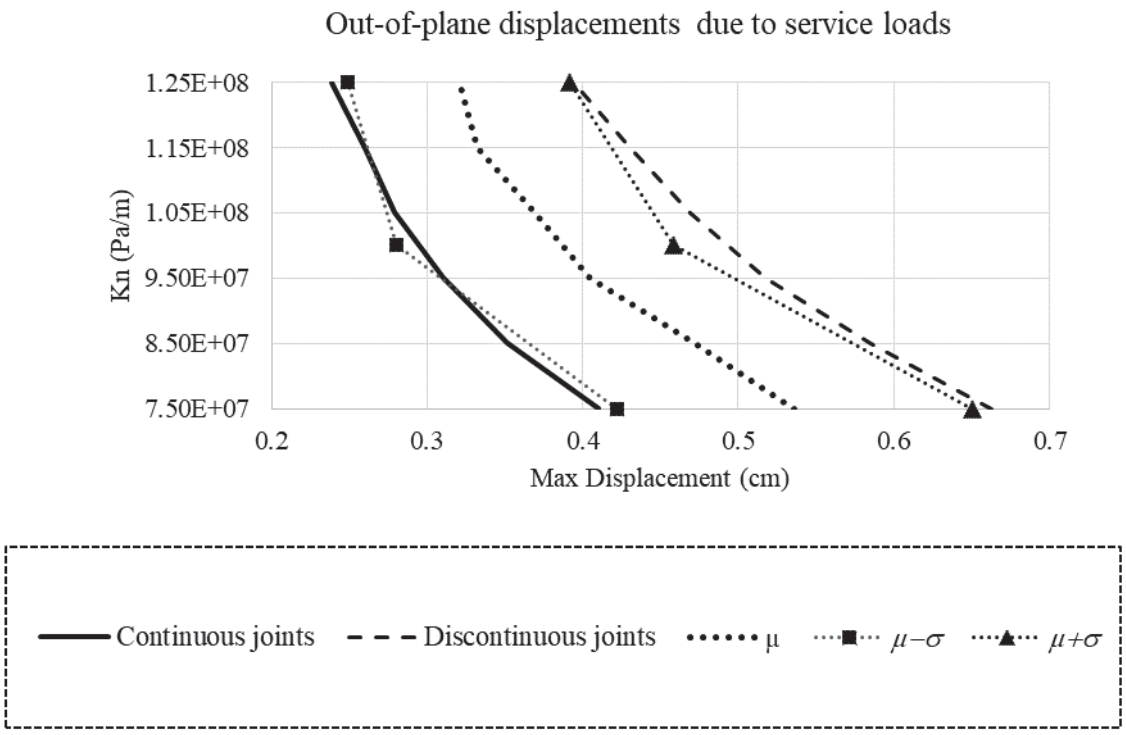

Figure 10: Parametric analysis of the normal joint stiffness in DSW

From these results, it can be stated that the model with discontinuous joints would overestimate -in most cases- the response of the walls with irregular joints subjected to trapezoidal loads. For the used *Kn*, the average value of the out-of-plane displacement of walls with irregular joints would be 25% lower than those of the model with discontinuous joints.

4.2. Effect of lateral constraint on the out-of-plane displacement

The DSW Length (L) / Height (H) ratio was analyzed for values from 1 to 6 and with intervals of 1 m. The models used were those from section 4.1 and using the software 3DEC. Figure 11 shows the relation between the structural response (drift) with the L/H ratio. It is observed that for L/H greater than 4, the restriction no longer influences the out-of-plane behavior.

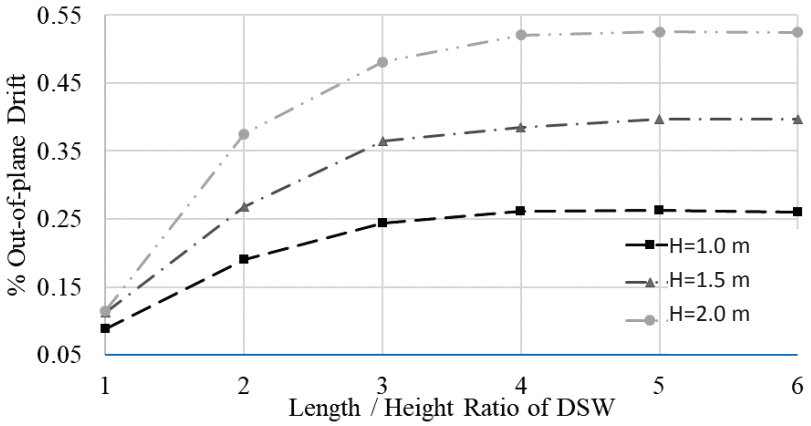

Figure 11: Variation of the out-of-plane drift to L/H ratio (Zanelli et al., 2019)

5. NUMERICAL MODELLING OF THE SCALED-DOWN MODELS

5.1. Selection of the type of discrete element for modelling the blocks

Since there are different types of discrete elements, the selection of the suitable element type should be based on the capability of the element for reproducing the equilibrium and the relative movement between the blocks, and on the computational time cost. In this section, the ability of three types of DEM elements to represent the units of the DSW and their respective computational cost is studied: spheres, clumps, and polyhedral. The numerical analyses will be done with the YADE program [24]. The three types of elements were modelled within a cube with a 0.40 m side. The loads are the gravity and, in some cases, a horizontal acceleration of 0.2g. In the constitutive model of Eq. 3 and 4, a null value of cohesion C was assumed.

The spheres are the element types with the simplest geometry to analyze in DEM algorithms, because the contact is a point and the normal direction to the contact plane is a known vector. However, the model with perfectly aligned spheres (Figure 12a) is unstable under any lateral load (Figure 12b). While the model with spheres assembled automatically (with the makeCloud command, Figure 12c) is unstable when applying the gravitational load (Figure

12d). In both cases, the frictional forces in contact zones are not enough to keep the arrangement stable.

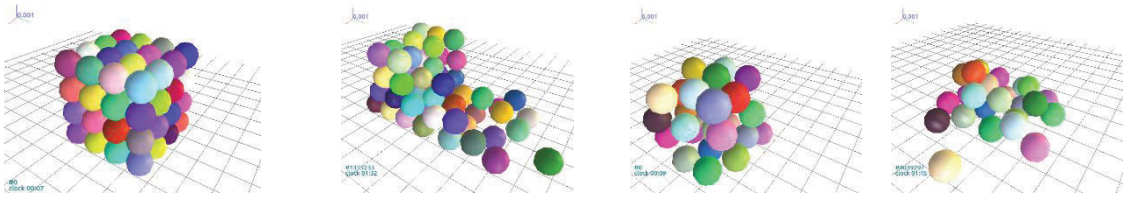

Figure 12: Numerical model with aligned spheres (a) before and after the application of gravity (b) after the application of a horizontal acceleration, (c) model of random spheres before the application of gravity, and (d) after the application of gravity

Clump elements are a group of rigid joined spheres that have the advantage to represent more complex element shapes and with more numerically stabilization than the spheres one. The types of clumps can be overlapped (Figures 13a and 13b) and without overlapping (Figures 13c and 13d). The shape of the overlapping clumps allows obtaining irregular elements that resemble the rounded blocks of some stone walls. Clump elements without overlapping could be used to represent walls with elements in a prismatic shape. In both cases, the overlapping and non-overlapping clumps, the stability of the models is due to the forces of the constitutive model and to the geometric interlocking of the elements, which depends on the diameter of the spheres.

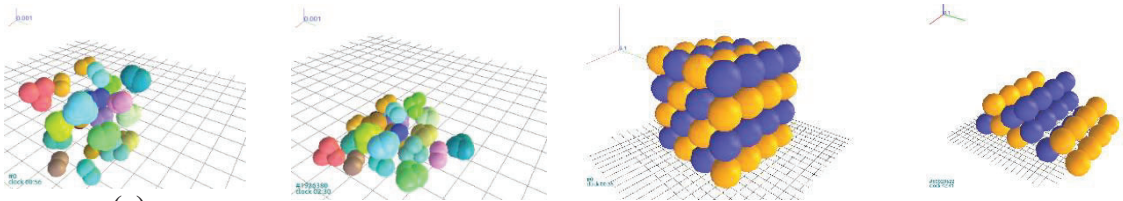

Figure 13: Numerical model: clumps with overlap (a) before and (b) after the application of gravity; and clumps without overlap (c) before and (d) after the application of a horizontal acceleration.

The polyhedron element can be regular or irregular. The regular polyhedron consists of a block of eight vertices. To create convex polyhedra, the command polyhedra_utils.polyhedra

was used, which allows defining the position of the centroid (Figure 14a). Before a lateral load, the blocks slide without rotating (Figure 14b). If the load increases, the slip is greater and the element may lose its stability and collapse. The numerical model with irregular polyhedra is generated with the polyhedra_utils.fillBox command, which fills a box with polyhedra without overlapping, of random geometry and various sizes (Figure 14c, 14d). This last model could represent the relative movement and rotation among the blocks of walls formed by irregular stone shapes.

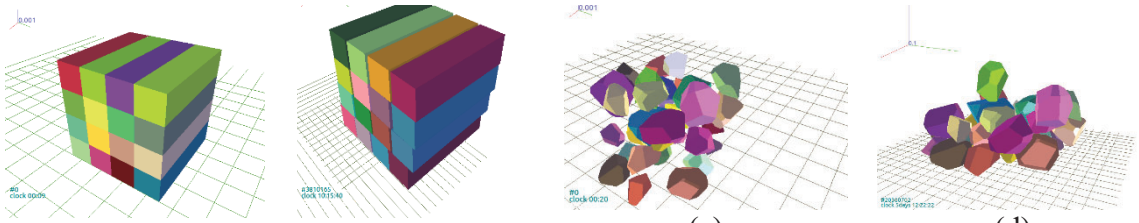

(a) (b) (c) (d)

Figure 14: Numerical model with regular polyhedra (a) before and (b) of the application of gravity. Numerical model with irregular polyhedra (c) before and (d) after applying gravity

For the analysis of the blocks, a computer with an Ubuntu 16.04 LTS operating system was used with 62.8 GB RAM and a 2.20 GHz processor. Table 6 shows the characteristics of the analyses for each type of element subjected to gravity and horizontal acceleration of 1 m/s2. The simulation ends automatically when the unbalanced force reaches 8%.

Table 6: Comparison of the analyses made with the four types of elements in Yade.

Element type	Sphere	Clumps with overlapping	Clumps without overlapping	Regular polyhedra *	Irregular polyhedra *
Number of elements	28	115	64	16	32
Time interval (s)	1.61E-06	1.10E-06	1.60E-06	1.00E-05	5.50E-06
Analysis speed (Hz)	60,000	19600	15,000	60	36
# cycles	23201001	10351204	131032001	5442249	2650924
Computational time	7’05’’	9’01’’	1h59’00’’	24h 05′0′′	+ 21h 12′55′′

(*) just under gravity loading

In summary, although the sphere model is the one with less computational time cost, it can be discarded as a model capable of representing the DSW under gravitational load due to its incapability to represent the contact forces in the walls. Overlapping clumps have a more stable balance than spheres due to the irregular shape of the blocks. This type of element has the advantage of being versatile in its geometry and of being of low computational cost. Non-overlapping clumps have a higher computational cost than overlapping clumps; however, they remain within reasonable ranges for academic purposes. Regular and irregular polyhedra have high computational costs since they needed more than 20 hours to reach equilibrium with the application of gravity. This is because the contact plane detection algorithms in the case of polyhedra are more complex than in the case of spheres and clumps. Therefore, the use of clump elements can be feasible to represent the behavior of the units of the CBL, SBR, and SBL walls.

5.2. Influence of Kn and ϕ parameters in the out-of-plane displacement

In this section, the out-of-plane displacement is analyzed as a function of *Kn and* ϕ from Eq. 2, and 3. For this, the CBL, SBL, and SBR walls described in section 2.1 were modelled in DEM, all with the same geometry, with typical values of *Kn* and ϕ found in the literature (see Table 6), $c = 0$ and $Ks = Kn / 2$. The models were implemented in YADE. The walls were modelled with clumps elements without overlapping, with dimensions approximated to the average of the blocks used in specimens and with discontinuous joints. Figure 15a shows a detail of the compact type assembly of the clumps in a lateral view, and Figure 15b shows the front view of a regular mesh type assembly. The compact type assembly allows spheres to have two contact points with the other two spheres that belong to a different clump, thus generating a geometric interlock.

The load application was pseudo-static, for which a damping of 0.8 was used. The elements were of the "FrictMat" type. The specific weight of the spheres was estimated at 3708 N/m^3, the weight of the model matches the weight of the tested wall (1371 N).

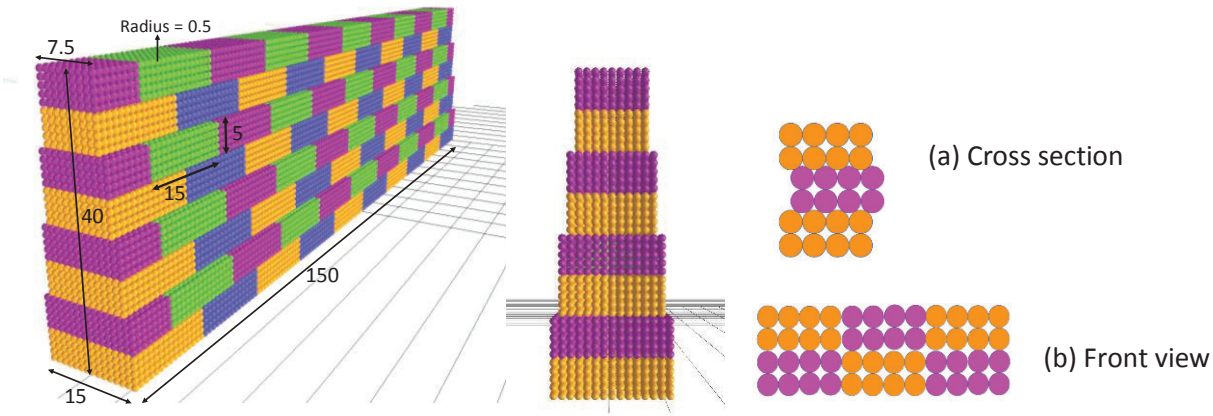

Figure 15: Scheme of the numerical model (dimensions in cm): (a) "Compact" type assembly and (b) "Regular mesh" type assembly.

SBL, CBL, and SBR wall models were subjected to loads corresponding to a 5° inclination of the tilting table (see section 2.2). Loads in the normal, FV, and out-of-plane, FH directions were simulated with Eq. 1; also, the out-of-plane displacement was estimated. *Kn* was varied from the minimum value that allows equilibrium to the value of 7.5e7 Pa/m. The value of ϕ ranged from 20 ° to 60 °. The results for ϕ = 20º are shown in Figure 16. It is observed that the SBL walls had a greater displacement than the SBR walls, for the same combination of joint parameters. Furthermore, the out-of-plane displacements decrease as the value of *Kn* increases. This is because, the greater the value of $Kn = 2Ks$, the tangential displacement of the joints will be less for the same force. Likewise, it was verified that the difference in results between an SBR wall and an SBL is less as *Kn* increases because when the stiffness is infinite, both curves tend to zero. The curves for the other values of ϕ follow the same trend.

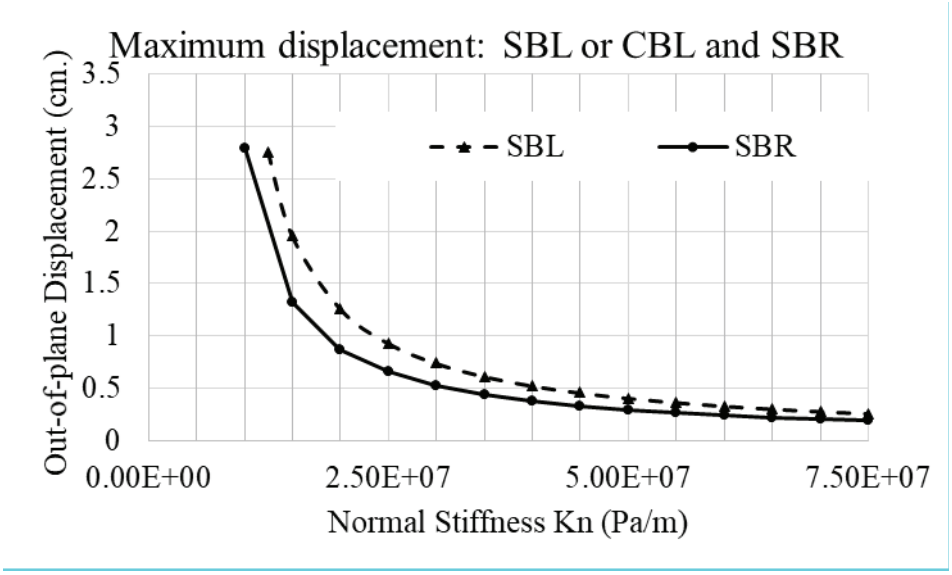

Figure 16: Influence of the Kn in the out-of-plane response for the wall models

5.3. Influence of Kn and ϕ parameters in the collapse angle

Using the same numerical model of section 3.4, the collapse angle (α_{max}) of each model was studied. This was obtained varying α from 0° until the model collapse. The tilting movement was done in intervals of 0.5°.

Table 7 presents the collapse angle values for the CBL, SBL, and SBR numerical models. It is verified that the collapse angle increases with the value of *Kn*, independently of the type of edges: free or restricted ones. The results of the SBL model show that for any value of *Kn*, the collapse angle remains constant for ϕ> 30 °. Since ϕ influences only the value of the maximum constitutive force (F^s_{max} , Eq. 3), the results indicate that for ϕ> 30 the contact forces (Fs, Eq. 2) generated in the SBL model are less than F^s_{max}. Therefore, the joint with ϕ> 30° keeps in elastic behavior state from the beginning of the inclination until the collapse of the wall. On the contrary, for the SBR model, the collapse angle increases as ϕ and *Kn* increase, which shows that the contact forces enter the nonlinear range. The friction force, F^s_{max}, is reached and the blocks are sliding for all the combinations of ϕ and *Kn* analyzed.

Table 7: Collapse angle $\alpha_{max,}$ for numerical models CBL or SBL and SBR

SBL or CBL	Kn (Pa/m)			SBR	Kn (Pa/m)		
ϕ	2.5x10^7	5.0x10^7	7.5x10^7	ϕ	2.5 x10^7	5.0 x10^7	7.5 x10^7
20°	10.0	13.5	14.5	**20°**	12.0	15.5	17.5
30°	11.5	14.5	16.0	**30°**	15.0	19.0	21.0
40°	11.5	14.5	16.0	**40°**	16.5	21.0	24.5
60°	11.5	14.5	16.0	**60°**	17.5	23.5	28.0

Figure 17a shows the overturning collapse mechanism of the CBL or SBL numerical model, while Figure 17b shows the bending failure of the SBR wall. The model in Figure 16a is capable of representing the CBL failure mechanism of Figure 5. However, the failure in the SBL specimen (Figure 6) has more erratic behavior due to the nature of the units. Figure 17b represents the failure mechanism of the SBR specimen shown in Figure 7.

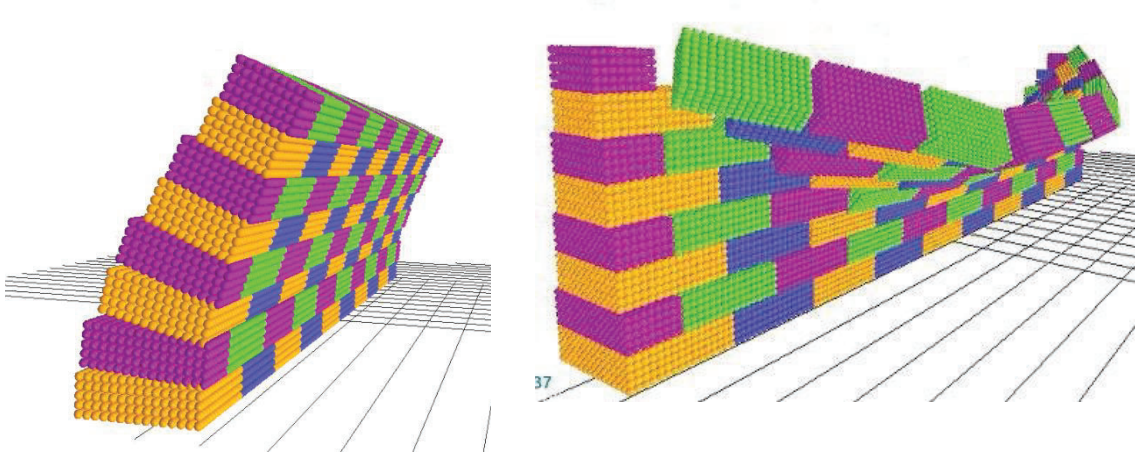

(a) (b)

Figure 17: Collapse of the models (a) CBL, SBL, and (b) SBR

The collapse mechanism of the CLB model (Figure 17a) is influenced by the geometric interlocking generated by the arrangement of the clump spheres (as seen in Figure 14a). According to Table 7, the collapse angle for CBL is independent of ϕ for values greater than 30 °. In this case, the collapse angle is determined by the dimensions of the blocks and the relative position of their centroid, which moves away from the axis as the angle α increases.

This behavior could be avoided with less slender sections and increasing the value of *Ks*. In the latter case, the displacements in the horizontal joints are smaller and the wall is more stable, then the collapse angle is greater. Table 7 shows how the collapse angle increases with *Kn*. When the values of *Kn* (or *Ks=0.5Kn*) and ϕ tend to infinity, the wall with no lateral restrictions will behave as a rigid block and the angle of collapse will tend to the value, $\alpha_{v,}$ = arctan (B/H) = 21.8º which corresponds to the collapse angle of a rigid block.

In the case of the SBR model, the lateral restrictions allow the generation of contact forces in the vertical joints caused by the catenary effect, which allows the elastic bending behavior of the wall. The collapse occurs when the maximum elastic displacement associated with F^s_{max} is reached, which depends on the value of the ϕ chosen.

From the point of view of the constitutive model, that SBR enters the inelastic range for ϕ greater than 30º, while SBL remains in the elastic range for the same inter particle friction angle. This is consistent with the fact that the maximum relative displacements before the collapse (*Un* and *Us* of Eq. 2) are greater in the SBR wall than in the SBL wall, as demonstrated in the tests and the numerical model.

5.4. Effect of the lateral restraint on the collapse angle

To analyze the effect of lateral restraint, the maximum shear forces were estimated in the models with free edges and restricted edges replacing α_{max} in Eq 1. The results, shown in Table 8, indicate that the lateral force value increases 38% on average due to the effect of lateral restraint. The effect of lateral constraints is greater as *Kn* and ϕ increase. This increment is similar to the one obtained in the experimental tests (35% on average) which shows the suitability of the numerical model to represent the lateral restrictions effect.

Table 8: Ratio of resistant lateral forces of models with restricted edges and with free edges

F_{VR}SBR/F_{VR}SBL	Kn (Pa/m)

ϕ	2.50E+07	5.00E+07	7.50E+07	Average = 1.38
20	1.20	1.14	1.20	Min = 1.14
30	1.30	1.30	1.30	Max = 1.70
40	1.42	1.43	1.50	S.D. = 0.17
60	1.51	1.59	1.70	V.C. = 12%

5.5 Calibration of Kn and ϕ parameters for the CBL, SBL, and SBR models

The *Kn* values of the CBL, SBL, and SBR models were obtained fitting the collapse angles of the DEM models (Table 7) with the experimental ones (Table 2). The value ϕ was obtained from a test on the tilting table using two stones with flat faces. The results of the calibration are shown in Table 9.

Table 9: Calibrated values for *Kn Ks* and ϕ

Kn (Pa/m)	*Ks* (Pa/m)	ϕ (°)	Material
5.0×10^7	2.5×10^7	35	Shale
1.75×10^8	0.86×10^8	32	Cobblestone

Table 10 shows some values found in the literature. We can see that the shale values are similar to those obtained by [19] for the limestone walls. Cobblestones values are similar to the granite reported by [37].

Table 10: *Kn* and ϕ parameters found in the literature

Kn (Pa/m)	*Ks* (Pa/m)	ϕ (°)	Material	Reference
1.0×10^9	1.0×10^9	32	Clay brick	[18]
5.00E+07	5.00E+07	25- 28	Schist	[19]
5.00E+07	5.00E+07	35-36	Limestone	[19]
1.00E+09	5.00E+08	41 - 45	Limestone	[42]
1.00E+08	2.50E+09	45	Granite	[42]
1.00E+09	5.00E+08	41 – 45	Granite	[43]

The numerical out-of-plane displacements, corresponding to the inclination of 5º, were calculated for the SBL and SBR walls and using the calibrated values of Table 9. Table 11 shows the comparison with the average values obtained experimentally. It is shown that there are differences of more than 50%. This indicates that the used DEM models do not reproduce

the out-of-plane displacement of SBL or SBR correctly but it seems a correct first approach with so simple academic particles to represent the real blocks of the test.

Table 11: Comparison of out-of-plane displacements

Out-of-plane displacement	Experimental	DEM	Difference
SBL	1.3 cm	0.4 cm	69%
SBR	0.2 cm	0.3 cm	50%

In this section, the numerical modeling of the scaled-down models has been reported. Results showed the influence of Kn and ϕ parameters (see sections 5.2 and 5.3). For all cases, the higher the Kn, the lower the out-of-plane displacement is. As expected, SBR's displacement values are less than SBL's ones for the same tilting angle and parameters. However, the average ultimate displacement of the SBR specimen is greater than the SBLs one, since SBR strength is greater than the corresponding to SBL. In case of SBR, results showed that the higher the ϕ, the higher the collapse angle is. In case of SBL, the collapse angle is independent of ϕ (for ϕ values greater than 30º) which indicates that the contact forces remain in the elastic domain (independent of ϕ according to Eq. 2) and the collapse mechanism would depend on the geometry (slenderness) of the block.

6. CONCLUSIONS

The analyzes carried out in this experimental and numerical work show that DEM methods are adequate to study and predict the failure mechanism and the collapse angle of stone walls subjected to out-of-plane loads. The models take into account the effect of the block's irregularity, the joint arrangement, and the boundary conditions. The results contribute to the state-of-the-art in DEM models to represent the behavior of DSW under out-of-plane loads.

The DEM models with a length/height ratio of 4 and restricted edges developed a bending collapse mechanism similar to that obtained experimentally in small-scale tests. This implies

that for these ratios, the effects of the edges are relevant. The collapse angle and the maximum out-of-plane displacements of the walls with constrained edges are greater than the displacements of the equivalent models with free edges, this is due to the effect of the catenary. The use of YADE clumps type elements allows simulations with low computational cost to regular or irregular DEM elements with reasonable results for a first approach. Further calculations varying the clump geometries need to be further explored.

Slender DEM models, with free edges and whose joints are governed by the Coulomb model, present overlapping collapse mechanisms due to the geometric instability of the wall. In this case, the failure angle will only depend on *Kn* (which defines the movement of the blocks) and not on ϕ (which defines the maximum resistant shear forces). For this reason, if this last value needs to be calibrated, then more robust models should be used to avoid geometric instability and to allow the increase of the shear forces in the joint.

From the DEM analysis, it is concluded that the use of discontinuous joints causes out-of-plane displacements around 25% greater than the displacements of the models with random irregular joints (as is the case of the majority of stone walls built without technical supervision). It is recommended to take this overestimation into account in case that it is desired to study walls with irregular blocks using numerical models with discontinuous joints.

The *Kn* and ϕ values of the Coulomb model- that fit the experimental results coincide with the values found in the literature. The *Kn* of the cobblestones is lower than the value of the wall made of stone. It is necessary to carry out more studies to establish typical values for different materials and shapes, and also validating the possibility to represent the blocks with other types of DEM elements. Further development will include full-scale specimens testing

to validate the numerical approach and to study different types of arrangements of the walls' blocks that correspond to actual practice in this type of constructions.

7. ACKNOWLEDGEMENTS

This research was developed under the support of the CONCYTEC with the contract N°109-2017-FONDECYT: "Validación de técnicas de construcción de pircas mediante estudios numérico-experimentales con tecnología desarrollada en Perú". The authors also thank to the University Grenoble-Alpes and Laboratory Soils Solids Structures and Risk for the use of 3DEC software during the stay of one of the authors in the laboratory at Grenoble.

8. REFERENCES

[1] Vincens E, Plassiard JP, Fry JJ. Dry Stone Retaining Structures. 1st ed.: Elsevier Ltd; 2016.

[2] Kendall A, Rodríguez A. Desarrollo y perspectivas de los sistemas de andenería de los andes centrales del Perú. Cusco: Institut Francais d'études Andines & Centro de Estudios Regionales Andinos Bartolomé de las Casas, Eds.; 2009.

[3] D'Ayala D, Speranza E. Definition of Collapse Mechanisms and Seismic Vulnerability of Historic Masonry Buildings. Earthquake Spectra. 2003;19(3):479-509. doi:10.1193/1.1599896

[4] Bothara, J, Brzev S. A Tutorial: Improving the Seismic Performance of Stone Masonry Buildings. EERI Publication Number WHE-2011-01; 2011.

[5] Colas A, Morel J, Garnier D. Yield design of dry- stone masonry retaining structures—Comparisons with analytical, numerical, and experimental data. International Journal for Numerical and Analytical Methods in Geomechanics 2008; 32(14): 1817-1832.

[6] Casapulla C, Cascini L, Portioli F, Landolfo R. 3D macro and micro-block models for limit analysis of out-of-plane loaded masonry walls with non-associative Coulomb friction. Meccanica 2014; 49(7):1653-78.

[7] Meyer P, Ochsendorf J, Germaine J, Kausel E. Earthquake Spectra 2007; 23(1): 77–94.

[8] De Buhan, Patrick, and Gianmarco De Felice. "A homogenization approach to the ultimate strength of brick masonry." Journal of the Mechanics and Physics of Solids 45.7 (1997): 1085-1104.

[9] Grillanda N., Chiozzi A., Milani G., Tralli A. Tilting plane tests for the ultimate shear capacity evaluation of perforated dry joint masonry panels. Part II: Numerical analyses. Engineering Structures 228, #111460(2021).

[10] Ceradini, V. (1992). Modellazione e sperimentazione per lo studio della struttura muraria storica. Ph. D. Thesis, University of Rome La Sapienza.

[11] Restrepo-Vélez, L y Magenes, G.. Static tests on dry stone masonry and evaluation of static collapse multipliers. Research Rep. ROSE 2009, 2, 72 pp.

[12] Milani G., Esquivel Y.W., Lourenço P.B., Riveiro B., Oliveira D.V. (2013). Characterization of the response of quasi-periodic masonry: Geometrical investigation, homogenization and application to the Guimarães castle, Portugal. Engineering Structures, 56, pp. 621-641.
[13] Milani G., Lourenço P.B. (2010). A simplified homogenized limit analysis model for randomly assembled blocks out-of-plane loaded. Computers & Structures, 88, pp. 690-717
[14] Cundall P, Strack O. The distinct numerical model for granular assemblies. Geotechnique 1979; 29: 47-65.
[15] Bui TT, Limam A, Sarhosis V. Discrete element modelling of the in-plane and out-of-plane behaviour of dry-joint masonry wall constructions. Engineering Structures 2017; 136: 277-294.
[16] Restrepo-Vélez L, Magenes G, Griffith M. Dry Stone Masonry Walls in Bending—Part I: Static Tests. International Journal of Architectural Heritage 2014, 8(1):1-28.
[17] Savalle N, Vincens É, Hans S. Experimental and numerical studies on scaled-down dry-joint retaining walls: Pseudo-static approach to quantify the resistance of a dry-joint brick retaining wall. Bull Earthquake Eng 2020; 18: 581–606.
[18] Quezada J, Vincens E, Mouterde R, Morel J. 3D failure of a scale-down dry stone retaining wall: A DEM modelling. Engineering Structures 2016; 117: 506-517.
[19] Oetomo J, Vincens E, Dedecker F, Morel J. Modeling the 2D behavior of dry- stone retaining walls by a fully discrete element method. International Journal for Numerical and Analytical Methods in Geomechanics 2016; 40(7): 1099-1120.
[20] Lemos, J.V., Campos, C.A., 2017. Simulation of shake table tests on out-of-plane masonry buildings. Part (V): discrete element approach. Int. J. Architect. Herit. 11 (1), 117 124.
[21] Sarhosis, V., Asteris, P., Wang, T., Hu, W., Han, Y., 2016a. On the stability of colonnade structural systems under static and dynamic loading conditions. Bull. Earthq. Eng. 14 (4),1131 1152.
[22] Sarhosis, V., Asteris, P.G., Mohebkhah, A., Xiao, J., Wang, T., 2016b. Three dimensional modelling of ancient colonnade structural systems subjected to harmonic and seismic loading. Struct. Eng. Mech. 60 (4), 633 653.
[23] Itasca Consulting Group. 3DEC - Three-dimensional distinct element code. Version 4.10, Minneapolis, MN; 2007.
[24] Kozicki J, Donze F. YADE - OPEN DEM: an open-source software using a discrete element method to simulate granular material. Engineering Computations 2008; 26(7): 786-805.
[25] Zanelli C, Santa-Cruz S, Daudon D. Evaluación de vulnerabilidad sísmica de Pircas mediante modelación numérica en Elementos Discretos: Aplicación al caso de las pircas en Carabayllo, Lima. Master thesis Pontificia Universidad Católica del Perú; 2019.
[26] Stockdale, Gabriel & Sarhosis, Vasilis & Milani, Gabriele (2020) Seismic capacity and multi-mechanism analysis for dry-stack masonry arches subjected to hinge control. Bulletin of Earthquake Engineering; 18. 10.1007/s10518-019-00583-7.
[27] McCombie PF, Mundell C, Heath A, Walker P. (2012) Drystone retaining walls: ductile engineering structures with tensile strength. Engineering Structures 2012; 45: 238-243.

[28] Moreau J. J., Jean M. Numerical treatment of contact and friction: the contact dynamics method. Engineering Systems Design and Analysis Conference, 1996, New York, United States. pp.201 - 208. ⟨hal-01825208⟩Dubois F. et al. 2011

[29] Dubois, F. & Jean, M. & Renouf, M. & Mozul, R. & Martin, Al. & Bagneris, M.. (2011). LMGC90. CSMA 2011 10e Colloque National en Calcul des Structures9-13 Mai 2011, Presqu'île de Giens (Var) https://hal.archives-ouvertes.fr/hal-00596875/document&usg=AOvVaw1On5YU_rIP5Se4ExZtshBf

[30] Isfeld A. Shrive N. Discrete Element Modeling of Stone Masonry Walls With Varying Core Conditions: Prince of Wales Fort Case Study; December 2014; International Journal of Architectural Heritage 9(5):141217131144002

[31] Chetouane, Brahim & Dubois, Frédéric & Vinches, Marc & Bohatier, Claude. (2005). NSCD discrete element method for modeling masonry structures. International Journal for Numerical Methods in Engineering. 64. 10.1002/nme.1358.

[32] Vinches M., A. Rafiee, C. Bohatier : Discrete element modeling of the mechanical behavior of ordinary houses and masonry structures, taking into account recorded earthquake accelerograms. Provence'2009, Seismic risk in moderate seismicity area from hazard to vulnerability, Aix-en-Provence, France, 6-8 juillet 2009

[33] Lemos, J. V. (2016). The Basis for Masonry Analysis with UDEC and 3DEC. In Sarhosis, V., Bagi, K., Lemos, J., & Milani, G. (Eds.), Computational Modeling of Masonry Structures Using the Discrete Element Method (pp. 61-89). IGI Global. http://doi:10.4018/978-1-5225-0231-9.ch003

[34] Lemos, J., (2007). Numerical issues in the representation of masonry structural dynamics with Discrete Elements. Proceedings of the 1st ECCOMAS Thematic Conference on Computational Methods in Structural Dynamics and Earthquake Engineer-ing (COMPDYN 2019), Papadrakakis, Fraiadakis (eds), Crete,Greece, 13–15 June, 1126.

[35] Lemos, J., (2017). Contact representation in rigid block models of masonry. International Journal of Masonry Research and In-novation 2, 321–334.

[36] Lemos, J., (2019). Discrete Element Modeling of the Seismic Behavior of Masonry Construction. Buildings 9 (43).

[37] Pulatsu, Bora & Bretas, Eduardo & Lourenco, Paulo. Discrete element modeling of masonry structures: Validation and application. Earthquakes and Structures. (2016). 11. 563-582. 10.12989/eas.2016.11.4.563

[38] Bui, T.-T., Limam, A., Sarhosis, V., Failure analysis of masonry wall panels subjected to in-plane and out-of-plane loading using the discrete element method. European Journal of Environmental and Civil Engineering. (2019) DOI: 10.1080/19648189.2018.1552897

[39] V. Sarhosis, K. Bagi, A.R. Lemos, G. Milani Computational Modeling of Masonry Structures Using the Discrete Element Method (2016) 978-1-5225-0231-9, IGI Global, Hershey, PA, USA

[40] V. Sarhosis, J.V. Lemos A detailed micro-modelling approach for the structural analysis of masonry assemblages Comput. Struct., 206 (2018), pp. 66-81, 10.1016/j.compstruc.2018.06.003

[41] Sarhosis, Vasilis & Forgács, Tamás & Lemos, Jose. (2020). Stochastic strength prediction of masonry structures: a methodological approach or a way forward?. RILEM Technical Letters. 4. 122-129. 10.21809/rilemtechlett.2019.100.

[42] Walker P, McCombie P, Claxton M. Plane strain numerical model for drystone retaining walls. Proceedings of the Institution of Civil Engineers-Geotechnical Engineering 2007; 160(2): 97-103.
[43] Harkness R, Powrie W, Zhang X, Brady K, O'Reilly M. Numerical modelling of full-scale tests on drystone masonry retaining walls. Géotechnique 2000; 50(2): 165-179.